Chapter 2

Numerical Study of Hypersonic Boundary Layer Receptivity Characteristics Due to Freestream Pulse Waves

Xiaojun Tang, Juan Yu, Tianli Hui,
Fenglong Yang and Wentao Yu

Additional information is available at the end of the chapter

http://dx.doi.org/10.5772/intechopen.70660

Abstract

A finite difference method is used to do direct numerical simulation (DNS) of hypersonic unsteady flowfield under the action of freestream pulse wave. The response of the hypersonic flowfield to freestream pulse wave is studied, and the generation and evolution characteristics of the boundary layer disturbance waves are discussed. The effects of the pulse wave types on the disturbance mode in the boundary layer are investigated. Results show that the freestream disturbance waves significantly change the shock standoff distance, the distribution of flowfield parameters and the thermodynamic state of boundary layer. In the nose area, the main disturbance modes in the boundary layer are distributed near the fundamental mode. With the evolution of disturbance along with streamwise, the main disturbance modes are transformed from the dominant state of the fundamental mode to the collective leadership state of the second order and the third order harmonic frequency. The intensity of bow shock has significant effects on both the fundamental mode and the harmonic modes in each order. The strong shear structure of boundary layer under different types of freestream pulse waves reveals different stability characteristics. The effects of different types of freestream pulse waves are significant on the distribution and evolution of disturbance modes. The narrowing of frequency band and the decreasing of main disturbance mode clusters exist in the boundary layer both for fast acoustic wave, slow acoustic wave and entropy wave.

Keywords: hypersonic flow, boundary layer, receptivity, pulse wave, numerical simulation

1. Introduction

With the progress that human achieved in the exploration of aviation and aerospace fields, the hypersonic vehicle technology has developed quickly. The design of hypersonic vehicle is a

complex problem based on hypersonic aerodynamics and involving multidisciplinary and multi-domain. Problems of hypersonic aerodynamics and aerodynamic heating, structures and materials technology are the main technological difficulties. There remains much variance between hypersonic flow and supersonic flow about the problem of aerodynamics. For the hypersonic boundary layer, entropy layer and shock wave layer overlapping each other, while it is high temperature and low density flow in boundary layer, which undoubtedly makes the hypersonic boundary layer flow more complex. Therefore, hypersonic aerodynamics is a key technology in the research and development of hypersonic vehicle. Various flow disturbance problems, usually exists in the flying environment of vehicle. For instance, the explosive blast wave [1], reverse jet [2, 3], the non-uniformity flow, the instability of flight, the rough wall and so on, which would happen in flying. It can be seen disturbances are common in flow fields. It's significantly different about the ideal hypothesis state of the steady flowfield and the flow condition existing in disturbance waves. The disturbance in the flowfield will have a significant influence on aerothermodynamics characteristics. The disturbance, whether it is strong or weak, will interfere with the flowfield, especially the shock and boundary layers. After the disturbance in the flowfield interference with shock wave and boundary layer, the disturbance wave will be induced. Then the induced wave will cause further interaction with boundary layer, and create new unstable waves. The stability characteristic of boundary layer and the laminar-turbulent transition mechanism will be significantly changed due to the induced unstable waves. Laminar-turbulent transition not only affects the aerodynamic heating of the wall of hypersonic vehicle, but directly changes the aerodynamic force. Especially, laminar-turbulent transition will greatly increases aerodynamic drag, which reduces the lift drag ratio of hypersonic vehicle significantly and increases the requirement of thermal protection.

Therefore, it is necessary to accurately predict the hypersonic unstable flowfield and the flowfield response characteristic induced disturbance waves during the design and development process of hypersonic aircraft. Considering the complexity and expensiveness of the hypersonic vehicle wind tunnel test, it is of practical significance to conduct the numerical simulation of hypersonic unsteady flowfield. In recent years, the hypersonic flowfield response induced by different disturbance waves and the influences of the disturbance wave on the stability of the boundary layer are studied by many scholars using numerical or experimental methods. Ma and Zhong [4] investigated the response of hypersonic boundary layer over a blunt cone to freestream acoustic waves at Mach 7.99. The receptivity of a flat plate boundary layer to a freestream axial vortex is discussed by Boiko [5]. Zhong [6] investigated the leading-edge receptivity to freestream disturbance waves for hypersonic flow over a parabola. The effect of wall disturbances on hypersonic flowfield, and the response of hypersonic boundary layer to wall disturbances are also widely studied [7–10]. Literature [11] points out that, after the interaction between any form of freestream disturbance and the shock wave as well as the boundary layer in hypersonic flow field, three independent forms of disturbance waves, including acoustic disturbance (fast and slow acoustic disturbance), entropy wave disturbance, and vortex wave disturbance will be generated. Among these investigations, most scholars are committed to study the effects of freestream continuous disturbance or the effects of wall disturbance on the stability of boundary layer and laminar-turbulent transition [12–14]. There is still less research on the effects of freestream pulse disturbance on the stability of boundary layer, and the mechanism in this field is still not fully understood. So, this paper

aims to study hypersonic flowfield and the stability characteristics of boundary layer under the freestream pulse wave. It should be mentioned that the significantly different showed in the influence mechanism of the wave types of continuous disturbance on the stability of boundary layer that had been pointed out by some scholars [6, 15, 16]. Ma and Zhong [15, 16] investigated the response of hypersonic plate boundary layer under different types of disturbance waves using direct numerical simulation and linear stability theory. It is found that acoustic disturbance has the greatest influence on the stability of boundary layer, and it is pointed out that the action mechanism of freestream entropy wave disturbance and vortex wave disturbance is similar to that of the fast acoustic wave disturbance, but different from the slow wave disturbance. Although it is significantly different between pulse disturbance wave and continuous disturbance wave in form, there is reason to believe that the response characteristics of hypersonic boundary layer are also significantly different under different freestream pulse waves. Therefore, the receptivity characteristics of hypersonic boundary layer under freestream pulse waves with different types are discussed in this paper.

In this investigation, the numerical simulations of hypersonic flowfield over a blunt wedge under the action of freestream pulse wave were conducted using a high order finite difference scheme. The response property of hypersonic flowfield under the action of freestream pulse wave analyzed, and the hypersonic boundary layer stability is investigated. The receptivity characteristic of hypersonic boundary layer under the action of different freestream pulse waves was compared, and the effects of the pulse wave types on the generation and evolution of the disturbance mode in the hypersonic boundary layer are discussed.

2. Basic equations and numerical method

2.1. Navier-Stokes equation

According to the forms of conservation equation, momentum equation and energy equation, the three basic equations of fluid governing equations can be written as a general form, that is, the two-dimensional unsteady compressive N-S equation can be expressed as:

$$\frac{\partial \mathbf{Q}}{\partial t}+\frac{\partial(\mathbf{f}\text{-}\mathbf{f}_v)}{\partial x}+\frac{\partial\left(\mathbf{g}\text{-}\mathbf{g}_v\right)}{\partial y}=0 \tag{1}$$

Where the state vector **Q** can be expressed as:

$$\mathbf{Q}=\left[\rho \;\; \rho u_x \;\; \rho u_y \;\; \rho E\right]^{\mathrm{T}} \tag{2}$$

Similarly, $\mathbf{f}$, $\mathbf{f_v}$, $\mathbf{g}$, $\mathbf{g_v}$ can be expressed respectively as:

$$\mathbf{f}=\left[\rho u_x \quad \rho {u_x}^2+P \quad \rho u_x u_y \quad \left(\rho E+P\right)u_x\right]^{\mathrm{T}} \tag{3}$$

$$\mathbf{f}_v=\left[0 \quad \tau_{xx} \quad \tau_{xy} \quad u_x\tau_{xx}+u_y\tau_{xy}+k\frac{\partial T}{\partial x}\right]^{\mathrm{T}} \tag{4}$$

$$\mathbf{g} = \begin{bmatrix} \rho u_y & \rho u_x u_y & \rho {u_y}^2 + p & (\rho E + p) u_y \end{bmatrix}^{\mathrm{T}} \tag{5}$$

$$\mathbf{g}_v = \begin{bmatrix} 0 & \tau_{xy} & \tau_{yy} & u_x \tau_{xy} + u_y \tau_{yy} + k \dfrac{\partial T}{\partial y} \end{bmatrix}^{T} \tag{6}$$

where u_x, u_y, P, ρ, T and E indicate the velocity in the x direction, the velocity in the y direction, pressure, density, temperature and total energy, respectively. k, $\boldsymbol{\tau}$ and E are the thermal conductivity, the stress component and the total energy, respectively.

2.2. Numerical method

In this paper, a high order finite difference method is used to solve the flowfield governing equation directly. The inviscid vector flux of the Navier-Stokes equation is divided into the positive and negative convection terms using S-W method [17]. The positive and negative convection terms are discretized by the 5th order upwind WENO scheme [18]. The viscous term is discretized by the 6th order central difference scheme [19]. In order to obtain the transient information of the flowfield and reduce computation time, the 3th TVD Runge-Kutta scheme is used for time advance [20].

The spatial discretization for positive and negative convection terms can be expressed as Eqs. (7) and (8), respectively:

$$W' = \left(m_1 W_{j+3} + m_2 W_{j+2} + m_3 W_{j+1} + m_4 W_j + m_5 W_{j-1} + m_6 W_{j-2} + m_7 W_{j-3} + m_8 W_{j-4}\right)/\Delta \tag{7}$$

$$H' = \left(n_1 H_{j+4} + n_2 H_{j+3} + n_3 H_{j+2} + n_4 H_{j+1} + n_5 H_j + n_6 H_{j-1} + n_7 H_{j-2} + n_8 H_{j-3}\right)/\Delta \tag{8}$$

where W and H are positive convection terms and negative convection terms, respectively; Δ is the grid spacing; W' and H' are the difference approximation of the derivative of W and H, respectively; m_i and n_i are specific coefficients, no longer list.

The spatial discretizations for viscous terms can be expressed as follow:

$$L' = \left(K_1\left(L_{j+1} - L_{j-1}\right) + K_2\left(L_{j+2} - L_{j-2}\right) + K_3\left(L_{j+3} - L_{j-3}\right)\right)/\Delta \tag{9}$$

where L, L', Δ and K_i are viscous terms, the difference approximation of the derivative of viscous terms, the grid spacing and specific coefficients, respectively, which are similar to the symbols in Eqs. (7) and (8).

The TVD Runge-Kutta discretization can be expressed as follows

$$\begin{cases} U^{(1)} = a_1 U^n + b_1 f^n \Delta t & U^{(2)} = a_2 U^n + b_2\left(U^{(1)} + f^1 \Delta t\right) \\ U^{(3)} = a_3 U^n + b_3\left(U^{(2)} + f^2 \Delta t\right) & U^{n+1} = U^{(3)} \end{cases} \tag{10}$$

where Δt is time increment for time advance; L(U) is the partial derivative of U relative to time.

http://dx.doi.org/10.5772/intechopen.70660

The variables a_i and b_i is the specific coefficients. b_1, b_2 and b_3 are equal to 1, 3/4 and 1/3, respectively; a_1, a_2 and a_3 are equal to 1, 1/4 and 2/3, respectively.

3. Computing model and conditions

The model parameters and calculation conditions of flowfield calculation includes the freestream condition, model parameter, boundary conditions and meshing. For freestream conditions, the freestream temperature is equal to 69 K, and the Mach number is equal to 6. The Reynolds number, based on the nose radius, is equal to 10,000. The angle of attack is equal to 0°. **Figure 1** shows the computing model and schematic diagram. Calculation mode is a blunt wedge with the wedge angle of 16°e; the nose radius r = 1 mm. the adiabatic wall, no-penetration and non-slip is introduced for wall condition; the symmetric boundary conditions is introduced for y = 0; the freestream conditions and exportation boundary conditions are introduced for the upstream of computing domain and the downstream of calculation domain, respectively. **Figure 2** shows the computational grid. The local intensive grid method is carried out near the nose area and wall area, and the grid number is 300 × 120. The parameters of blunt wedge nose radius r, freestream velocity V_∞, freestream temperature T_∞, freestream viscosity coefficient μ_∞, freestream conductivity coefficient k_∞, freestream density ρ_∞ are chosen as the normalized basic measure that is the characteristic variable.

In order to explore the influence of freestream pulse wave on hypersonic flow field, the interaction process between freestream pulse slow acoustic wave and hypersonic flowfield is direct numerical simulated. In present investigation, the stable flow over a blunt wedge at Mach 6 is calculated firstly, and then the simulation of hypersonic unsteady flowfield under the freestream pulse wave is conducted by introducing freestream pulse slow acoustic wave at the upstream boundary of computing domain.

The introducing time of the freestream pulse wave is recorded as t = 0. The form of pulse slow acoustic wave is expressed as follows:

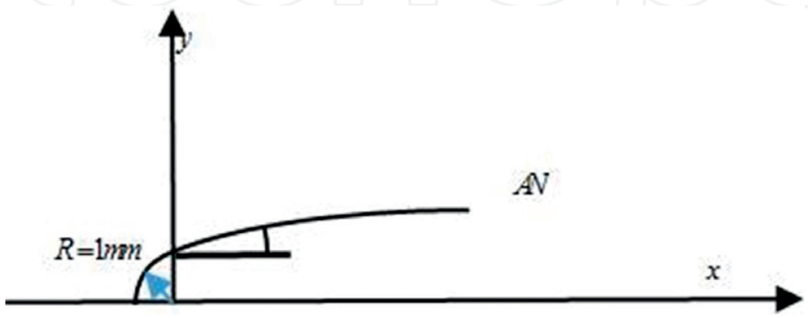

Figure 1. Computational model and schematic diagram.

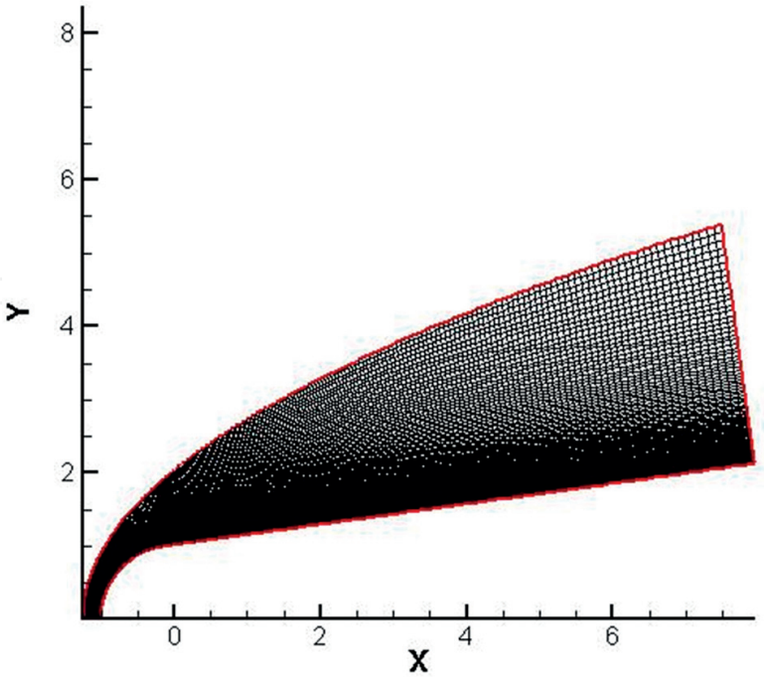

Figure 2. Mesh grid.

$$\begin{bmatrix} u' \\ v' \\ p' \\ \rho' \end{bmatrix} = \begin{cases} [0 \;\; 0 \;\; 0 \;\; 0]^T & (t < 0) \\ \left[A \;\; 0 \;\; -\frac{A}{M_\infty} \;\; -AM_\infty\right]^T e^{i\left(kx - \frac{F\mathrm{Re}}{10^6}t + \frac{\pi}{2}\right)} & (0 \le t < 2) \\ [0 \;\; 0 \;\; 0 \;\; 0]^T & (t \ge 2) \end{cases} \tag{11}$$

Where u', v', P' and ρ' indicate the velocity disturbance along x direction, the velocity disturbance along y direction, the pressure disturbance and the density disturbance, respectively; A indicates the amplitude, F indicates the generalized frequency, t indicates time. Here, $A = 8 \times 10^{-2}$; $k = 3.1446 \times 10^{-4}$; $F = 50\pi$; $Ma_\infty = 6$.

4. Results and discussion

4.1. Response of the hypersonic flowfield to freestream pulse wave

4.1.1. Response of the hypersonic flowfield

Before analyzing, it should be pointed out that the numerical simulation method and the grid independence in present work is validated in our previous investigation [21–23], which indicates the numerical method adopted in this paper is reliable. **Figure 5** shows the contours of pressure under freestream pulse wave at different times.

Figure 3(a)–(d) in the figure correspond to t = 2.0, 4.0, 6.0 and 8.0, respectively. In **Figure 3**, when the pulse wave enters the flow field, it first interacts with the bow-shaped shock wave. When it is encountered with the slow acoustic pulse wave, the bow-shaped shock wave is

http://dx.doi.org/10.5772/intechopen.70660

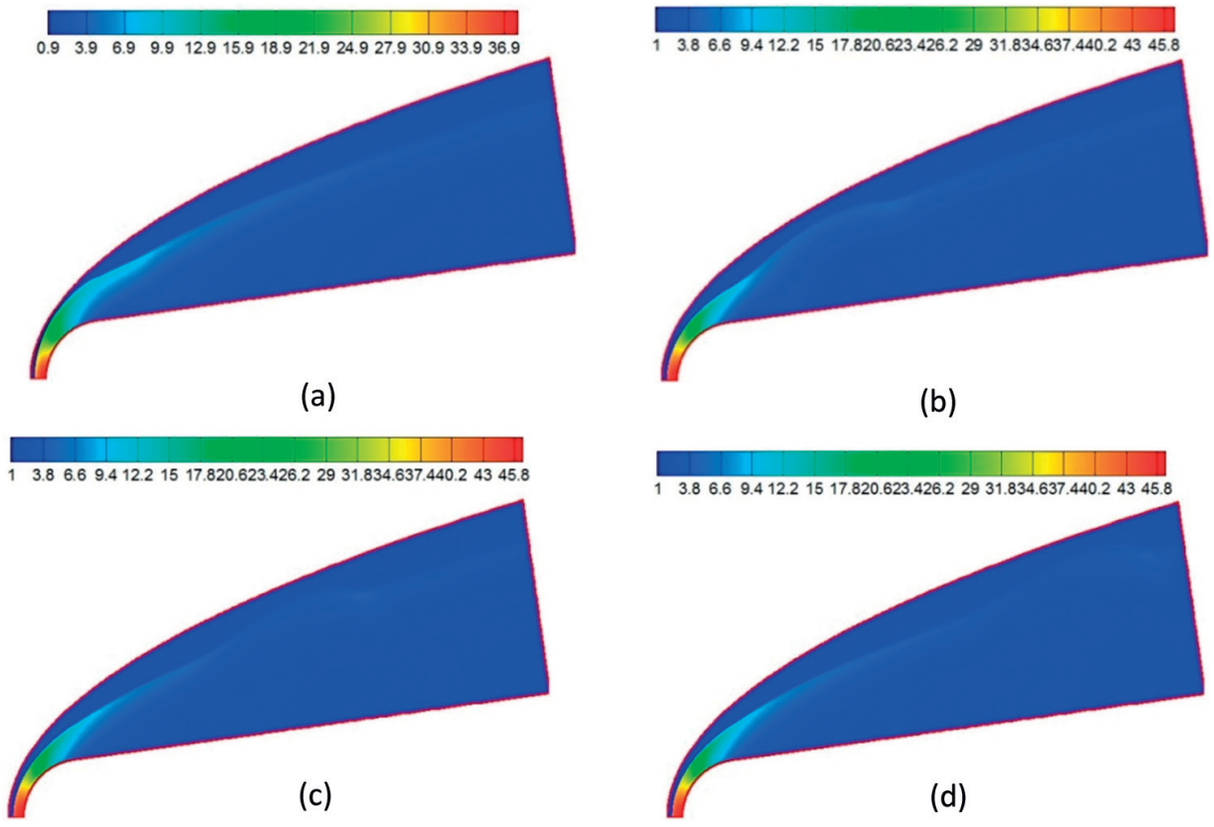

Figure 3. Contours of pressure under freestream pulse wave at different times. (a) *t*=2.0, (b)) t=4.0, (c)*t*=6.0, (d)) *t*=8.0.

deformed and protruded outward, and the surrounding pressure is also significantly affected. Due to the deformation of the shock wave, the pressure of outward convex region near shock wave is significantly increased, and the flowfield pressure below the bow shock wave is greatly reduced. That is to say, from **Figure 3(a)–(d)**, it shows that the freestream disturbance waves significantly interact with the bow-shaped shock waves, which greatly changes the shock standoff distance and the distribution of flowfield pressure in the active region.

Figure 4 shows the contours of density under freestream pulse wave at different times. **Figure 4(a)–(f)** correspond to t = 0.0, 2.0, 4.0, 6.0, 8.0 and 10.0, respectively. **Figure 5** shows the contours of temperature under freestream pulse wave at different times. **Figure 5(a)–(f)** correspond to t = 0.0, 2.0, 4.0, 6.0, 8.0 and 10.0, respectively. As can be seen from **Figure 4**, the pulse wave disturbance has a great impact on the density. The density of the flowfield changes significantly under the action of freestream pulse wave, especially in the disturbance area between the pulse wave and the bow-shaped shock wave, where the density of the region is significantly smaller. Compared with the significant changes of flowfield density around the shock wave, the pulse wave has much smaller effect on the density in the boundary layer. Meanwhile, the closer to the nasal area, the greater the density changes and the effects are after the action of pulse wave. Obviously, this is because the closer the bow-shaped shock wave is to the nose area, the stronger the action is. Therefore, it can be concluded that the stronger the intensity of the shock wave is, the more intense the effect of the pulse slow acoustic wave and the bow-shaped shock wave are. As can be seen from

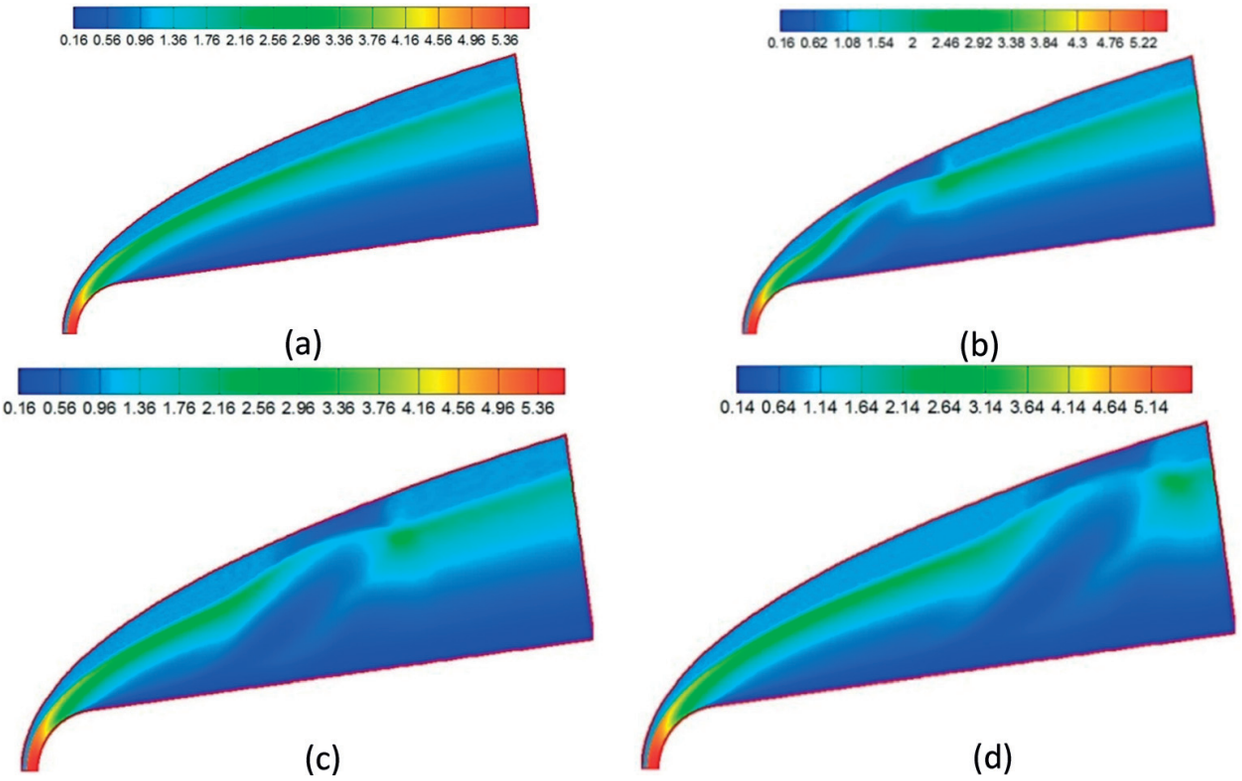

Figure 4. Contours of density under freestream pulse wave at different times. (a) t=0.0, (b) t=4.0, (c) t=6.0, (d) t=8.0.

Figure 5, the effect of disturbances on the temperature is pretty significant, which similar to the density. Under the action of impulse disturbances, a strip area exists in the hypersonic flowfield temperature disturbances between the boundary layer and the shock wave, which is similar to the change trend of the flowfield density's disturbances. What is worth noting is that from the upstream to the downstream, the strip area becomes longer; this is due to the fact that through the shock wave, the disturbance wave slows down. The farther it is away from the wall, the greater the flow velocity is, which leads to the disturbance wave's different spread velocity to the downstream. It also can be seen from **Figure 5** that the temperature in the boundary layer is much more significantly affected by the pulse wave compared with the temperature change of the flowfield near the shock wave. That is to say, the freestream pulse wave's influence on the thermodynamic state in boundary layer is significantly greater than that on the thermodynamic state the outside boundary layer. It is known that the temperature is a characteristic parameter of the thermodynamic properties in the boundary layer. Obviously, the freestream pulse disturbance wave changes the thermal mechanism of the strong shear flow in the boundary layer, while the thermodynamic mechanism is considered to have an important effect on the stability of the boundary layer [24], so it is reasonable to believe that the pulse slow acoustic wave in freestream plays a considerable role in the stability of hypersonic boundary layer.

Figure 6 shows the contours of velocity along axis y under freestream pulse wave at different times. From **Figure 6**, under the action of the pulse slow acoustic wave, the velocity in the interference area between pulse wave and shock wave, the flowfield between the boundary

http://dx.doi.org/10.5772/intechopen.70660

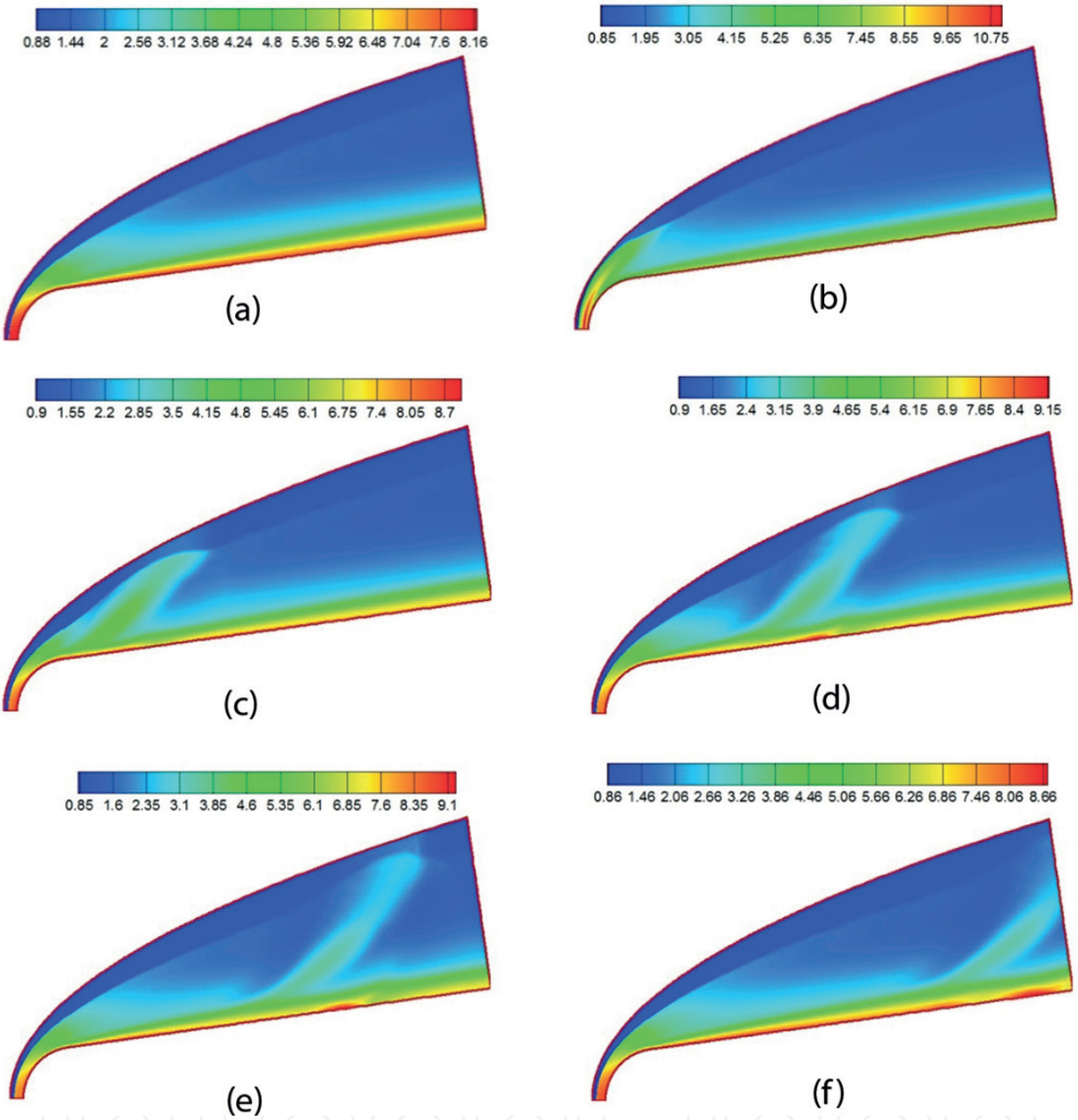

Figure 5. Contours of temperature under freestream pulse wave at different times. (a) t=0.0, (b) t=2.0, (c) t=4.0, (d) t=6.0, (e) t=8.0, (f) t=10.0.

layer and shock wave, and the flowfield in the boundary layer change greatly. On the other hand, the velocity disturbance modes out of the boundary layer and the velocity disturbance modes near the boundary layer differ significantly. From **Figure 6**, there are many obvious disturbance characteristic regions in the hypersonic boundary layer under the action of freestream pulse disturbances. It can also be seen that the boundary layer's disturbance velocity is very large, which shows that there is complex interference in the boundary layer under the action of the pulse wave. It is worth mentioning that, after the disturbance wave interfering with the bow-shaped shock wave, and entering into the flowfield, a part of the

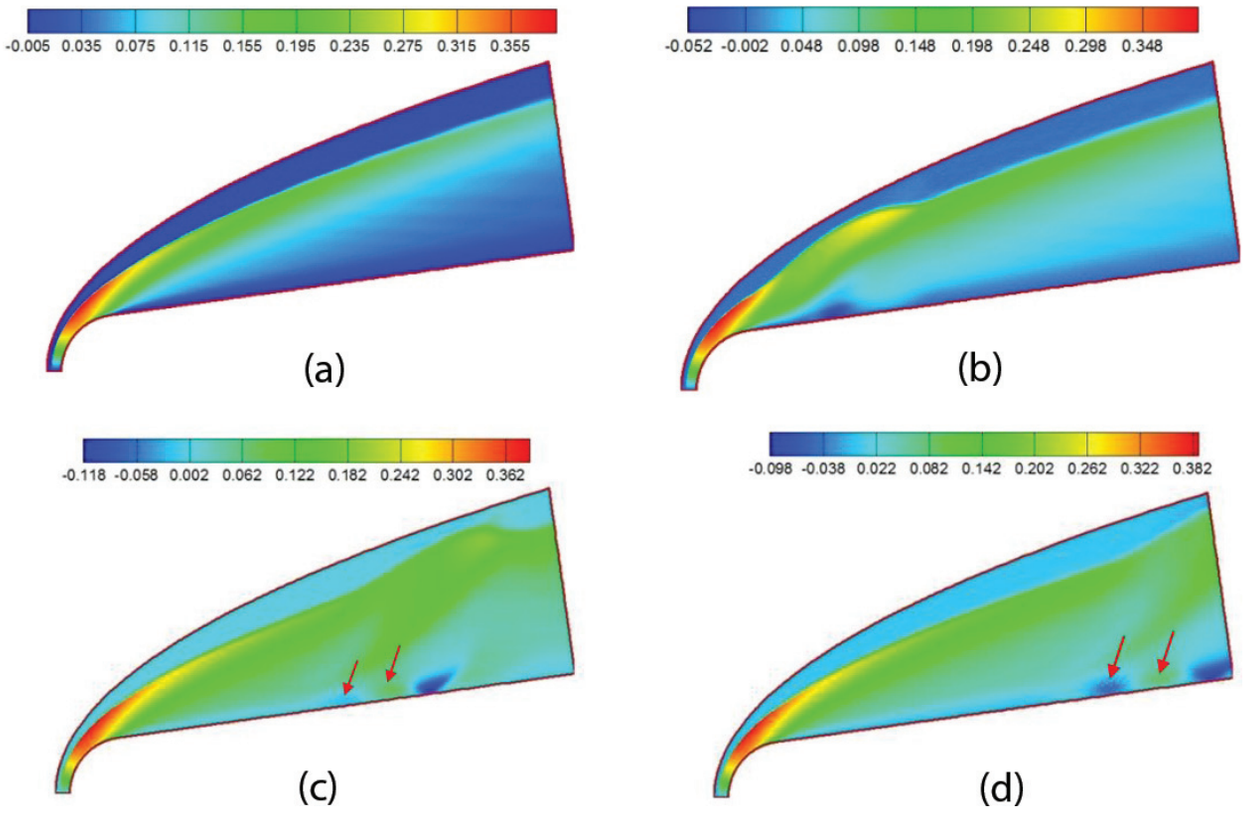

Figure 6. Contours of velocity along axis *y* under freestream pulse wave at different times. (a) *t*=0.0, (b) *t*=4.0, (c) *t*=8.0, (d) *t*=10.0.

wave will propagate from the upstream to the downstream of the flowfield and a part of the reflected wave will oscillate between the shock wave and the wall [24]. Moreover, the velocity disturbance mode in the boundary layer becomes more complicated on account of reflected waves. As shown in **Figure 6(c)** and **(d)**, the disturbance characteristic regions marked with arrows are induced by the reflected waves in the flowfield.

4.1.2. Response of the boundary layer

Figure 7 shows the distribution of friction factor disturbance on wall under freestream pulse wave at different times (t = 2.0, 4.0, 6.0, 8.0, 10.0). It can be seen from the figure that, when the pulse wave disturbance is through some place of the wall, the friction factor reduces at first, and after reaching a minimum value, it increases. When the pulse disturbance completely passes this point, the disturbance effect on this position is not over, and it will go through a number of processes in oscillating changes like getting bigger-smaller-bigger-smaller, until the change magnitude decreases to zero. It is clear that this oscillating decreasing phenomenon is caused by the reciprocating reflected waves between the wall and the bow shock. Most importantly, the friction factor is an important parameter for characterizing the shear flow, which indicates that the strong shear flow structure in the boundary layer under freestream pulse wave has changed.

Figure 8 shows the comparisons of the density, temperature and pressure disturbances on wall at different times. **Figure 8** indicates that, under freestream pulse wave, the variations of the

http://dx.doi.org/10.5772/intechopen.70660

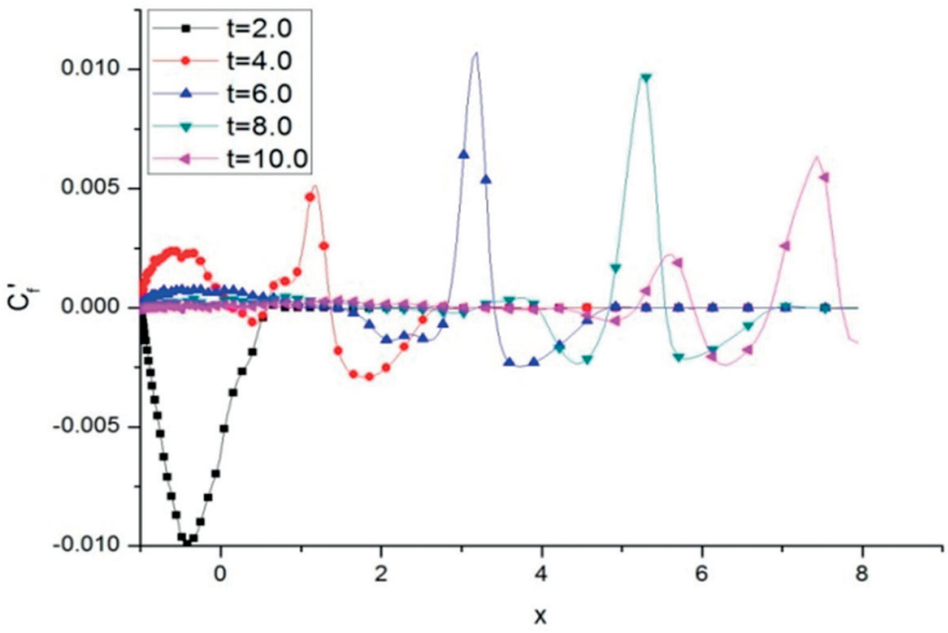

Figure 7. Distribution of friction factor disturbance on wall under freestream pulse wave at different times.

density, temperature and pressure disturbances on wall are similar to that of friction factor. Zhang et al. [19] studied the evolution of continuous small disturbance in hypersonic flow using direct numerical simulation (DNS), and found that, because of the normal shock wave, the forcing disturbance in freestream is enlarged. From **Figure 8**, it is obtained that the

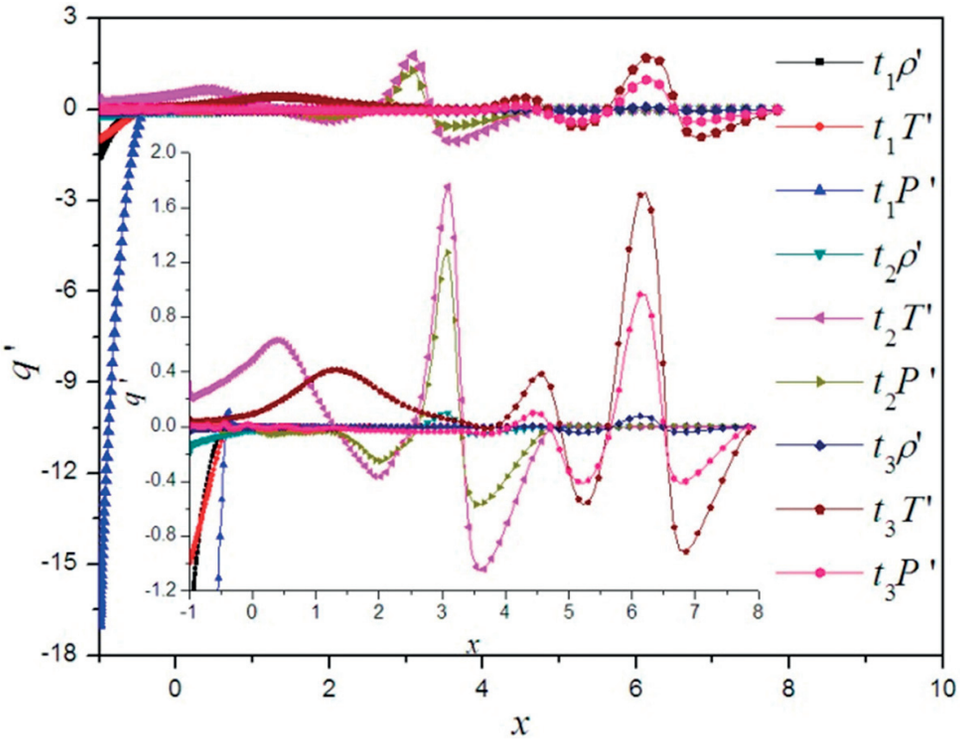

Figure 8. Comparison of the density, temperature and pressure disturbances on wall at different times ($t_1 = 1.0$, $t_2 = 6.0$, $t_3 = 9.0$).

amplitude of parameters disturbance on the wall is enlarged sharply relative to that of initial wave in freestream. The numerical results agree with Li's results. It also shows that the disturbance amplitudes of pressure on the nose of blunt wedge are larger than that on non-nose, and the former are several times, even more than 10 times, larger than the latter; while the discrepancy is tiny for temperature and density.

To study the evolution of the disturbance wave in boundary layer during the interaction process, the temperature disturbance on wall along the streamwise is considered. **Figure 9** shows the distribution of temperature disturbance on wall along the streamwise at $t = 8.6$. As discussed earlier, it has been verified that the disturbance amplitude of aerothermodynamics parameters will undergo a damped oscillation during the interaction process although there is just a half sinusoidal pulse wave in freestream. **Figure 9** indicates that the distance between crests as well as trough of disturbance variables changed markedly during the damped oscillation process. The distances a1-a2, a2-a3, b1-b2 and b2-b3 along the x-axis direction equal to 1.733, 2.939, 1.541 and 1.491, respectively. Hence, it is obvious that the damped oscillation is aperiodic. In other word, the waves with other frequencies are induced due to the interaction between freestream blast wave and bow shock wave as well as boundary layer. It should be noted that the evolution of the wave's modes in the blunt wedge boundary layer exerts an important impact on both boundary layer stability characteristic and laminar-turbulent transition [10, 25]. There is little research focused on the evolution of the wave's modes in the boundary layer under freestream pulse wave, and the evolution characteristic remains unclear although a host of in-depth researches is done in the evolution of the wave's modes in boundary layer under freestream continuous small disturbances in recent years.

To analyze the disturbance mode distribution in the hypersonic boundary layer and its evolution characteristics along the streamwise under the action of freestream pulse wave, the fast Fourier transformation method is used to decode the time domain signal of the

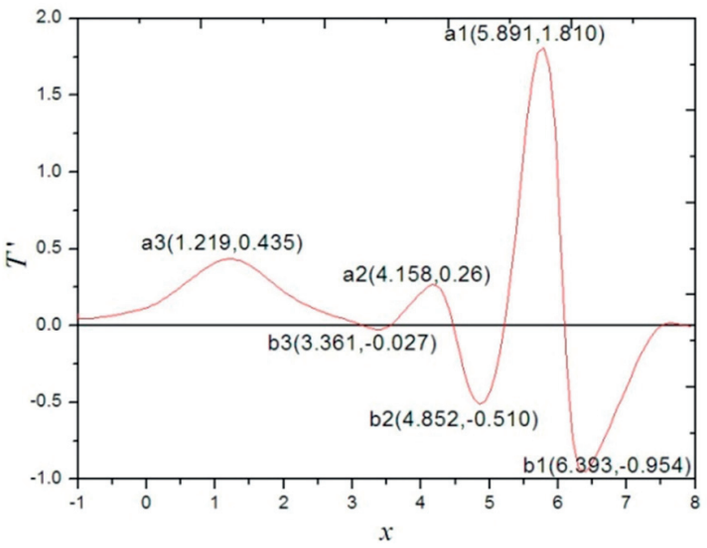

Figure 9. Temperature disturbance profile along streamwise at $t = 8.6$.

http://dx.doi.org/10.5772/intechopen.70660

boundary layer disturbance. Furthermore, the signals are expanded in frequency order to make it as a frequency function, thereby converting the time domain signal of the pressure disturbance into a frequency domain signal. **Figure 10** shows the results of the Fourier frequency spectral analysis of pressure disturbance in boundary layer under freestream pulse wave at different locations. **Figure 10(a)–(d)** are the results of the Fourier frequency spectral analysis when $x = 0.83566$, $x = 1.2196$, $x = 3.3050$ and $x = 5.3846$, respectively. It can be seen from **Figure 10(a)** that, at the location of x = 0.83566, namely the nose area, the main disturbance modes in the boundary layer are distributed near $f = 0.25$, indicating that near the fundamental frequency, the disturbance mode component of other frequencies is relatively small, which is consistent with the results obtained by Zhang et al. [19] in studying continuous waves. It also shows that the higher the disturbance mode's frequency is, the smaller its component ratio will be. Based on **Figure 10(b)**, at the position of x = 1.2196, the disturbance mode component ratio near the fundamental frequency decreases rapidly, the high frequency disturbance harmonic mode like the second order harmonic frequency and above significantly increase. And the main disturbance modes in the boundary layer are distributed near $f = 0.5$, that is near the second order harmonic frequency. The main

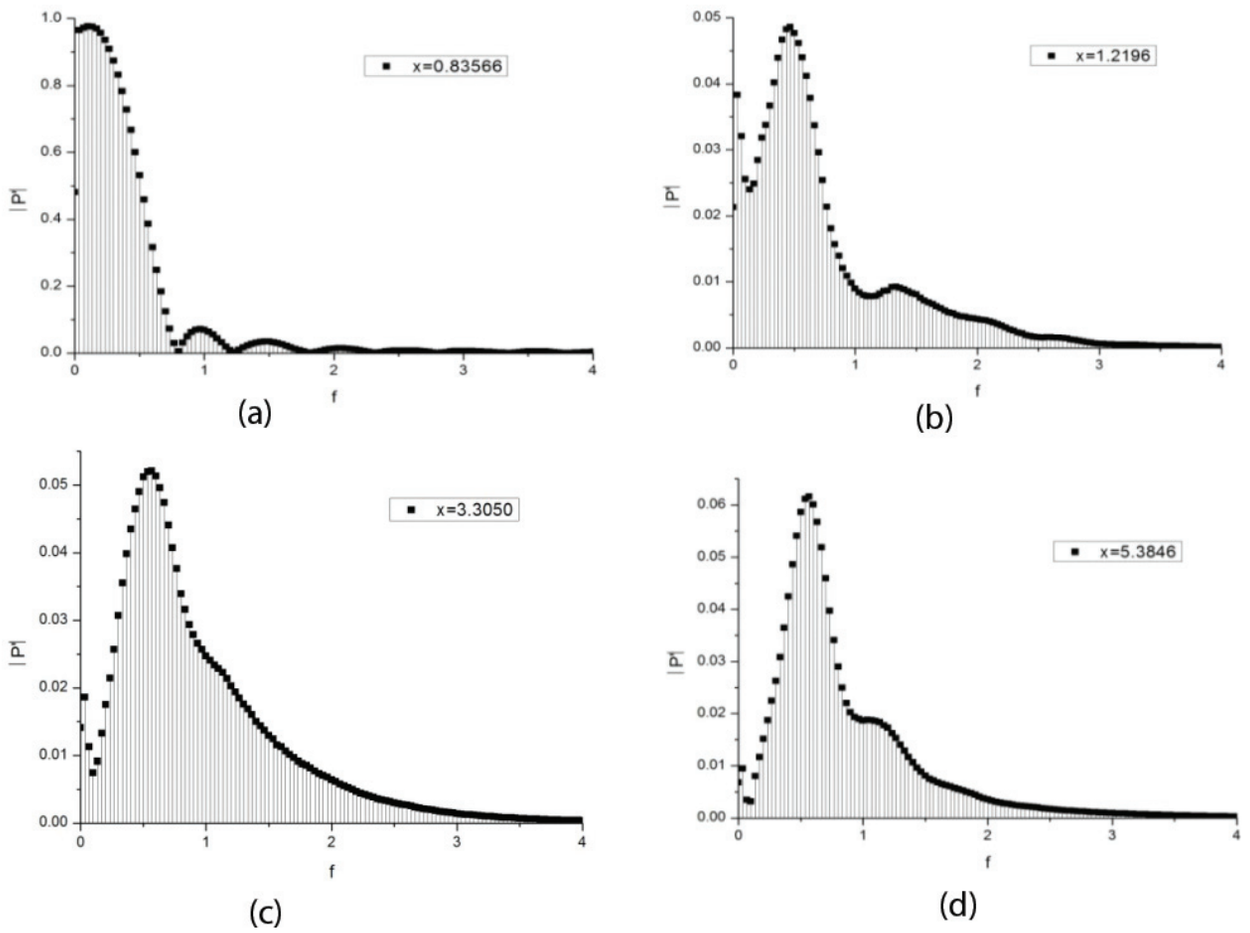

Figure 10. Fourier frequency spectral analysis of pressure disturbance in boundary layer under freestream pulse wave at different locations. (a) x=0.83566, (b)x=1.2196, (c) x=3.3050, (d) x=5.3846.

disturbance modes in the boundary layer migrate from the fundamental frequency to the second order harmonic frequency. In **Figure 10(c)**, it can be seen that at the position of x = 3.3050, the disturbance mode components in the vicinity of the fundamental frequency are further reduced, and the proportion of disturbance mode components is further increased. The main disturbance modes in the boundary layer are distributed at f = 0.5–0.75, namely near the second and third order harmonic frequency. The main disturbance modes in the boundary layer are transformed from the dominant state of the second order harmonic frequency to the collective leadership state of the second order harmonic frequency and the third order harmonic frequency. According to **Figure 10(d)**, at the position of x = 5.3846, the distribution of the boundary layer disturbance modes is similar to that at x = 3.3050. The main disturbance modes in the boundary layer are distributed near the second and third order harmonic frequency, but the frequency band of the boundary layer disturbance mode is significantly narrowed.

Figure 11 shows the evolution of different disturbance modes along streamwise in boundary layer. **Figure 11(a)–(f)** are the evolution of the fundamental frequency mode, the second order harmonic frequency, the third order harmonic frequency, the fourth order harmonic frequency, the fifth order harmonic frequency and the sixth order harmonic frequency, respectively. From **Figure 11(a)**, in the nose region, the amplitude of the fundamental frequency becomes smaller. When out of the nose region, the amplitude of the fundamental frequency gradually becomes smaller and generally remains. In **Figure 11(b)**, it can be seen that in the nose region, the amplitude of the second order harmonic frequency mode significantly becomes smaller. Out of the nose region, the amplitude of the second order harmonic frequency mode continues to increase. From **Figure 11(c)**, it can be seen that the amplitude of the third order harmonic frequency mode becomes smaller in the nose region, and the third order harmonic frequency mode first increases and then decreases in the downstream evolution. From **Figure 11(d)–(f)**, it shows that the evolution of the fourth order harmonic frequency mode, the fifth order harmonic frequency mode and the sixth order harmonic frequency mode along the streamwise is similar to that of the third order harmonic frequency mode. As shown in the figure, whether it is the fundamental mode or harmonic modes, in the area of the nose boundary layer, the amplitude of the disturbance significantly becomes smaller, indicating that the intensity of the bow shock in the hypersonic flowfield becomes weak, and it has significant effects on both the fundamental mode and the harmonic modes in each order. According to the figure, it also shows that except for the fundamental mode, from the nose area to the non-nose area, the amplitude of each harmonic frequency mode all increase significantly. It is believed that this phenomenon is caused by the recompression of the flowfield, which means in this region, the effect of the shock wave intensity on the harmonic frequency modes of the boundary layer is smaller than the recompression effect, and the effect of the shock wave intensity on the fundamental mode of the boundary layer is larger than the recompression effect.

4.2. Effects of pulse wave type

In this section, to discuss the effects of the pulse wave types on the generation and evolution of the disturbance mode in the hypersonic boundary layer, the numerical simulations of hypersonic flowfield under the action of freestream pulse fast acoustic wave, slow acoustic wave and

http://dx.doi.org/10.5772/intechopen.70660

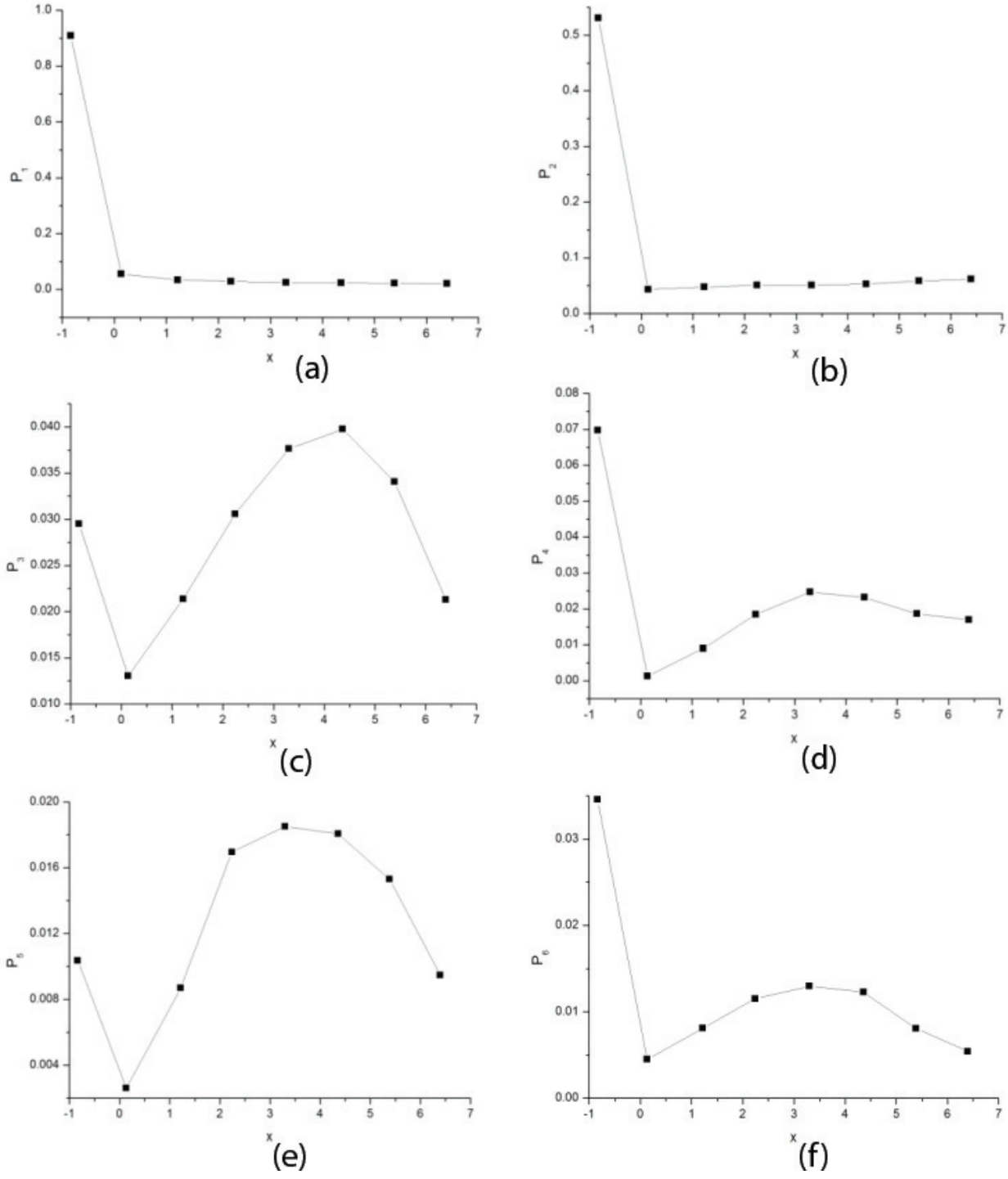

Figure 11. Evolution of different disturbance modes along streamwise in boundary layer. (a) P_1, (b) P_2, (c) P_3, (d) P_4, (e) P_5, (f) P_6.

entropy wave were conducted. It should be noted that the wall temperature $T_w = 200$ K, and the amplitude $A = 6 \times 10^{-2}$. The other computational condition is consistent with Section 4. The forms of pulse fast acoustic wave and entropy wave is no longer listed in this section. Due to the fact that the wall of shear force is decided by the friction factor on wall directly which is a key

parameters for representing the strong shear structure in boundary layer, the stability of the hypersonic boundary layer is the study of the stability of the strong shear structure. **Figure 12** shows the distribution of friction factor disturbance on wall under different freestream pulse waves at $t = 6$. From **Figure 12**, it is obtained that, under freestream pulse waves, the mainstream disturbance wave influence on the wall friction coefficient under the pulse slow acoustic wave is opposite to that under pulse fast acoustic wave and entropy wave. There is significant difference between the disturbance amplitude of the wall friction coefficient under pulse fast acoustic wave and that under entropy wave. It also can be seen that there is a significant difference in the friction factor disturbance on wall caused by the reflected wave for these three cases, and the reflected wave has a significant effect on the friction factor. In general, different types of freestream pulse waves have different effects on the friction factor on wall, which indicates the interaction between the strong shear structure of boundary layer and different types of freestream pulse waves have different mechanisms of action. That is, the strong shear structure of boundary layer under the action of different types of freestream pulse waves reveals different stability characteristics.

Figure 13 shows the pressure disturbance in boundary layer under different freestream pulse waves. **Figure 13(a)** and **(b)** are corresponding the position $s = 0.92619$ and 5.90498, respectively. From **Figure 13**, it can be seen that the pressure disturbance in boundary layer under the action of different types of freestream pulse waves appear different changes in the time domain.

The Fourier frequency spectral analysis of pressure disturbance in boundary layer under different freestream pulse waves is shown in **Figure 14**. **Figure 14(a)–(c)** are corresponding the position $s = 0.92619$, $s = 3.83551$ and $s = 8.02802$, respectively. **Figure 14** shows that the

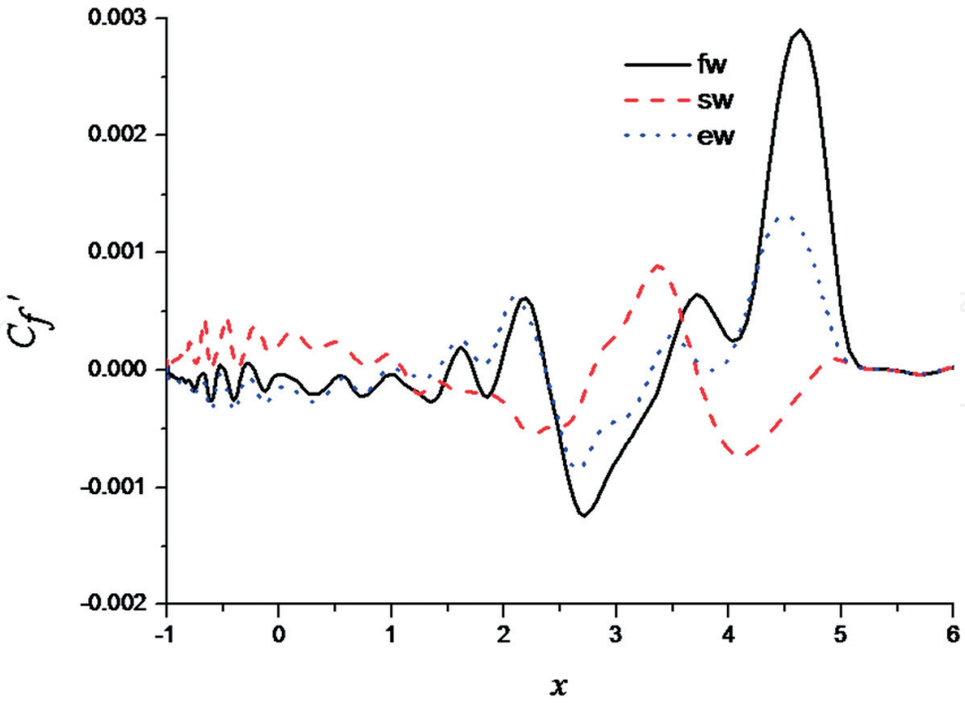

Figure 12. Distribution of friction factor disturbance on wall under different freestream pulse waves at t = 6 s.

http://dx.doi.org/10.5772/intechopen.70660

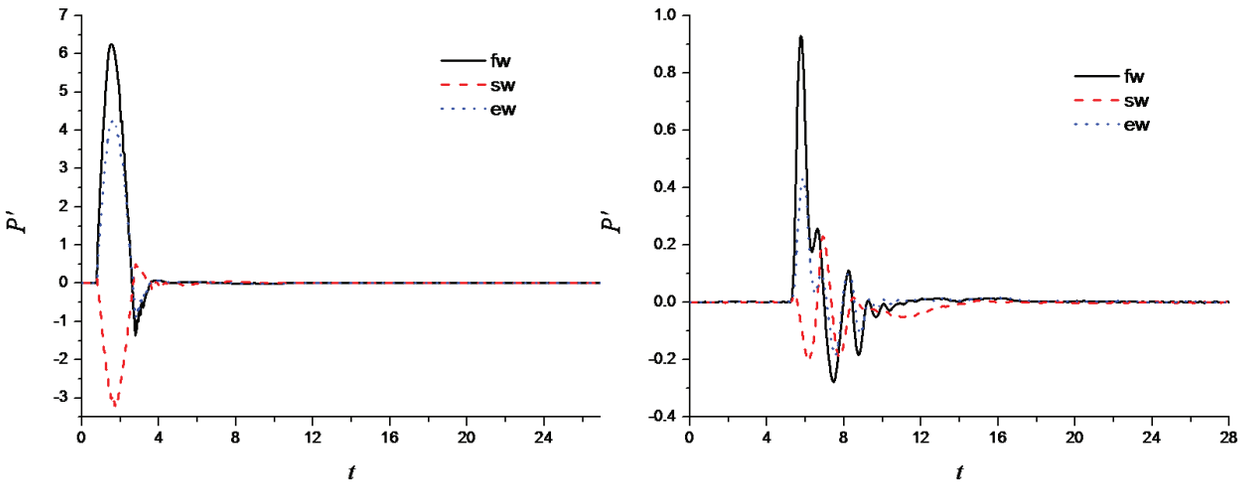

Figure 13. Pressure disturbance in boundary layer under different freestream pulse waves. (a) *s*=0.92619, (b) *s*=5.90498.

effects of different types of freestream pulse waves are significant on the distribution of modes in boundary layer and the evolution of disturbance modes along with the streamwise. From the figure, it is obtained that, s = 0.92619, the Fourier frequency spectral curve of pressure disturbance in boundary layer under different freestream pulse waves shows similar trend. Namely, the max amplitude of the disturbance modes in boundary layer are distributed near f = 0.25, and four main disturbance clusters (near f = 0.25, 1.0, 1.5 and 2.0) exist in the hypersonic boundary layer both for all cases. With evolution of disturbance waves in boundary layer along with the streamwise, at s = 3.83551, four main disturbance clusters still exist in the hypersonic boundary layer both for fast acoustic wave and entropy wave. However, the distribution of the four main disturbance clusters changes sharply, which indicates there is movement of main disturbance clusters in the boundary layer. It also can be seen that, at s = 3.83551, there is only one main disturbance cluster (near f = 0.5) in the hypersonic boundary layer for slow acoustic wave, and the other main modes have a remarkable decline. It is obtained that, at s = 8.02802, the number of main disturbance mode clusters in the boundary layer both for fast acoustic wave and entropy wave decreases

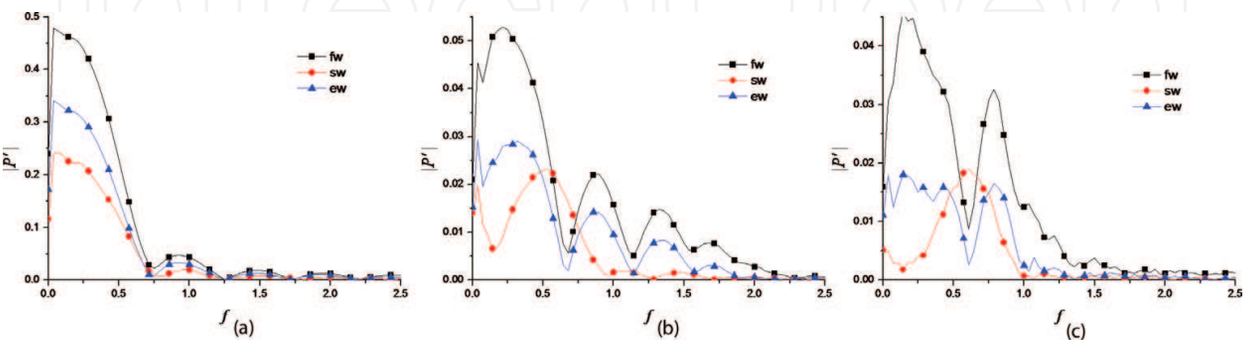

Figure 14. Fourier frequency spectral analysis of pressure disturbance in boundary layer under different freestream pulse waves. (a) s = 0.92619, (b) s = 3.83551, (c) s = 8.02802.

sharply. In general, the narrowing of frequency band and the decreasing of main disturbance mode clusters exist in the boundary layer both for all cases.

5. Conclusions

In present study, a finite difference DNS method is used to investigate the response of the hypersonic flow field to freestream pulse wave, and the generation and evolution characteristics of the disturbance mode in the hypersonic boundary layer are analyzed. The effects of the pulse wave types on the generation and evolution of the disturbance mode in the hypersonic boundary layer are investigated. The study drew the conclusions as follow:

1. The freestream disturbance waves significantly interact with the bow-shaped shock waves, which greatly changes the shock standoff distance and the distribution of flowfield parameters in the active region. The stronger the intensity of the shock wave is, the more intense the effect of the freestream pulse slow acoustic wave and the bow-shaped shock wave are. The freestream pulse wave's influence on the thermodynamic state in boundary layer is significantly greater than that on the thermodynamic state the outside boundary layer. There are many obvious disturbance characteristic regions in the hypersonic boundary layer under the action of freestream pulse disturbances. There is complex interference in the boundary layer under the action of the pulse wave.

2. In the nose area, the main disturbance modes in the boundary layer are distributed near the fundamental frequency, and the disturbance mode component of other frequencies is relatively small. In the nose area, the disturbance mode component ratio near the fundamental frequency decreases rapidly, the high frequency disturbance harmonic mode like the second order harmonic frequency and above significantly increases. With the evolution of the disturbance waves in the boundary layer from the upstream to the downstream, the main disturbance modes in the boundary layer are transformed from the dominant state of the fundamental frequency to the collective leadership state of the second order harmonic frequency and the third order harmonic frequency. The intensity of the bow shock in the hypersonic flowfield has significant effects on both the fundamental mode and the harmonic modes in each order. From the nose area to the non-nose area, the effect of the shock wave intensity on the harmonic frequency modes in the boundary layer is less than the recompression effect, and the effect of the shock wave intensity on the fundamental mode in the boundary layer is larger than the recompression effect.

3. The interaction between the strong shear structure of boundary layer and different types of freestream pulse waves have different mechanisms of action. The strong shear structure of boundary layer under the action of different types of freestream pulse waves reveals different stability characteristics. The effects of different types of freestream pulse waves are significant on the distribution of modes in boundary layer and the evolution of disturbance modes along with the streamwise. The narrowing of frequency band and the decreasing of main disturbance mode clusters exist in the boundary layer both for freestream pulse fast acoustic wave, slow acoustic wave and entropy wave.

http://dx.doi.org/10.5772/intechopen.70660

Author details

Xiaojun Tang[1]*, Juan Yu[2], Tianli Hui[1], Fenglong Yang[1] and Wentao Yu[1]

*Address all correspondence to: tangxiaojun2214@163.com

1 Beijing Spacecrafts, China Academy of Space Technology, Beijing, China

2 China Center for Information Industry Development, Beijing, China

References

[1] Pierce HB, Manning JC. Experimental Investigation of Blast Loading on an Airfoil in Mach Number of 0.7 Airflow with Initial Angle-of-Attack Change of 20. NASA Resport, 1963, NASA-TN-D-2876.

[2] Aso S, Hayashi K, Mizoguchi M. A study on aerodynamic heating reduction due to opposing jet in hypersonic flow. AIAA Paper. 2002;**2002**:646

[3] Hayashi K, Aso S, Tani Y. Numerical study on aerodynamic heating reduction by opposing jet. Memoirs of the Faculty of Engineering. 2006;**66**(1):39-54

[4] Ma YB, Zhong XL. Boundary-layer receptivity of Mach 7.99 Flow over a blunt cone to free-stream acoustic waves. Journal of Fluid Mechanics. 2006;**556**:55-103

[5] Boiko AV. Receptivity of a flat plate boundary layer to a free stream axial vortex. European Journal of Mechanics - B/Fluids. 2002;**21**:325-340

[6] Zhong X. Leading-edge receptivity to free stream disturbance waves for hypersonic flow over a parabola. Journal of Fluid Mechanics. 2001;**441**:315-367

[7] Fedorov AV, Khokhlov AP. Receptivity of hypersonic boundary layer to wall disturbances. Theoretical and Computational Fluid Dynamics. 2002;**15**:231-254

[8] Tumin A, Wang X, Zhong X. Numerical simulation and theoretical analysis of perturbations in hypersonic boundary layers. AIAA Journal. 2011;**49**(3):463-471

[9] Wang X, Zhong X, Ma Y. Response of a hypersonic boundary layer to wall blowing–suction. AIAA Journal. 2011;**49**(7):1336-1353

[10] Egorov IV, Fedorov AV, Sudakov VG. Direct numerical simulation of disturbances generated by periodic suction-blowing in a hypersonic boundary layer. Theoretical and Computational Fluid Dynamics. 2006;**20**(1):41-54

[11] Kovasznay LSG. Turbulence in supersonic flow. Journal of Aeronautical Sciences. 1953;**20**: 657-682

[12] P. Balakumar. Receptivity of supersonic boundary layers due to acoustic disturbances over blunt cones. 37th AIAA Fluid Dynamics Conference and Exhibit; American Institute of Aeronautics and Astronautics, Miami, Florida; Reston, VA: 2007

[13] Kara K, Balakumar P, Kandil OA. Effects of nose bluntness on hypersonic boundary-layer receptivity and stability over cones. AIAA Journal. 2011;**49**(12):593-2606

[14] Xin-Liang LI, De-Xun FU, Yan-Wen MA, et al. Acoustic calculation for supersonic turbulent boundary layer flow. Chinese Physical Society. 2009;**26**(9):181-184

[15] Ma Y, Zhong X. Receptivity of a supersonic boundary layer over a flat plate, part 2: Receptivity to Freestream sound. Journal of Fluid Mechanics. 2003;**488**(6):79-121

[16] Ma Y, Zhong X. Receptivity of a supersonic boundary layer over a flat plate, part 3: Effects of different types of free-stream disturbances. Journal of Fluid Mechanics. 2005;**532**(6):63-109

[17] Steger J, Warming RF. Flux vector splitting of the in-viscid gasdynamic equations with application to finite difference methods. Journal of Computational Physics. 1981;**40**:263-293

[18] Liu XD, Osher S, Chan T. Weighted essentially non-oscillatory schemes. Journal of Computational Physics. 1994;**115**:200-212

[19] Zhang Y, Fu D, Ma Y, Li X. Receptivity to free-stream disturbance waves for hypersonic flow over a blunt cone. Science in China Series G: Physics, Mechanics & Astronomy. 2008;**51**(11):1682-1690

[20] Shu CW. Essentially Non-Oscillatory and Weighted Essentially Non-Oscillatory Schemes for Hyperbolic Conservation Laws. NASA/CR-97-206253

[21] Tang X, Zhu X, Hui T, et al. Receptivity characteristics of a hypersonic boundary layer under freestream slow acoustic wave with different amplitudes. European Physical Journal Applied Physics. 2017;**79**:31101-1-31101-15

[22] Tang X, Lv H, Meng X, Wang Z, Lv Q. Stability characteristic of hypersonic flow over a blunt wedge under freestream pulse wave. Central. European Journal of Physics. 2014;**12**(1): 17-31

[23] Wang Z, Tang X, Lv H, Shi J. Temporal and spatial evolution characteristics of disturbance wave in a hypersonic boundary layer due to single-frequency entropy disturbance. The Scientific World Journal. 2014;**39**(2):359-371. DOI: 10.1155/2014/517242

[24] Xian L, Li XL, Fu DX, Ma YW. Effects of wall temperature on boundary layer stability over a blunt cone at Mach 7.99. Computers & Fluids. 2010;**39**:359-371

[25] Saric WS, Reed HL, Kerschen EJ. Boundary-layer receptivity to freestream disturbances. Annual Review of Fluid Mechanics. 2002;**34**:291-319